ANNUAL REVIEWS Further
Click here for quick links to Annual Reviews content online, including:
• Other articles in this volume
• Top cited articles
• Top downloaded articles
• Our comprehensive search

Annu. Rev. Nucl. Part. Sci. 2013.63:383-405. Downloaded from www.annualreviews.org
Access provided by WIB6380 - Gesellschaft fur Schwerionenforschung on 11/10/20. For personal use only.

Search for Superheavy Nuclei

J.H. Hamilton,[1] S. Hofmann,[2] and Y.T. Oganessian[3]

[1]Department of Physics and Astronomy, Vanderbilt University, Nashville, Tennessee 37235; email: j.h.hamilton@vanderbilt.edu

[2]GSI Helmholtzzentrum für Schwerionenforschung, 64291 Darmstadt, Germany; email: s.hofmann@gsi.de

[3]Flerov Laboratory of Nuclear Reactions, Joint Institute for Nuclear Research, 141980 Dubna, Moscow Region, Russia; email: oganessian@jinr.ru

Annu. Rev. Nucl. Part. Sci. 2013. 63:383–405

The *Annual Review of Nuclear and Particle Science* is online at nucl.annualreviews.org

This article's doi: 10.1146/annurev-nucl-102912-144535

Copyright © 2013 by Annual Reviews. All rights reserved

Keywords

superheavy nuclei, magic numbers for protons and neutrons, α decay, spontaneous fission

Abstract

We describe the discoveries of new superheavy nuclei (*a*) with Z = 107–112 produced in cold fusion reactions between ^{208}Pb and ^{209}Bi and beams of A > 50 and (*b*) with Z = 113–118 in hot fusion reactions between actinide nuclei and ^{48}Ca. We also discuss the facilities used in these measurements. We compare the behavior of the α-decay energies and half-lives, spontaneous fission half-lives, cross sections, and excitation functions with expectations from theoretical calculations. Finally, we outline future research directions, including studies of the detailed properties of nuclei synthesized at higher yields, searches for new elements with Z = 119 and 120, and developments of new facilities.

Annu. Rev. Nucl. Part. Sci. 2013.63:383-405. Downloaded from www.annualreviews.org
Access provided by WIB6380 - Gesellschaft fur Schwerionenforschung on 11/10/20. For personal use only.

Contents

1. INTRODUCTION

A fundamental question that has long intrigued scientists is: What are the limits of elements that can be found in nature or produced in the laboratory? By 1935, the periodic table of elements was complete—ranging from hydrogen (Z = 1) to uranium (Z = 92)—except for Z = 43 and 61. By 1945, these two elements had been discovered, along with neptunium (Z = 93) and plutonium (Z = 94). During the next two decades, new elements up to Z = 100 were discovered.

In 1949, the nuclear shell model was introduced to explain the special stability of nuclei with Z and N (number of neutrons) equal to 2, 8, 20, 28, 50, 82, and 126 (the last for N only). For these numbers, protons and neutrons form filled, closed shells in which there is a large gap in the single-particle energies to the next available shell, just as electrons have closed shells for the noble gases. Nuclei such as $^{4}_{2}He_2$, $^{16}_{8}O_8$, $^{40}_{20}Ca_{20}$, $^{48}_{20}Ca_{28}$, and $^{208}_{82}Pb_{126}$ are spherical doubly magic; both their protons and neutrons form closed shells. Given that N = 126 was magic, would Z = 126 be magic, providing special stability to nuclei with Z = 126? The Z limit for the existence of a superheavy nucleus (SHN) is reached when the barrier against spontaneous fission (SF), B_f, goes to zero (B_f = 0 MeV). Then, the nucleus splits into two fragments at a timescale $T_{SF} \approx 10^{-19}$ s. In the macroscopic approach (the charged liquid drop model, for example), SF already dominates

in nuclei with $Z^2/A \geq 39$ (where A is the atomic weight), providing a limit on the existence of nuclei immediately after $Z \approx 100$, where B_f vanishes. However, the charged liquid drop model cannot explain the almost constant fission barrier heights in actinide nuclei ranging from uranium to fermium ($B_f \approx 6$ MeV). Strutinsky (1) introduced a microscopic correction for the proton and neutron shell fillings that explained these fission barriers and the existence of elements beyond $Z = 100$. Calculations performed in the 1960s predicted the existence of a so-called island of stability associated with spherical shell closures at $N = 184$ and $Z = 114$, but not $Z = 126$ (**Figure 1**) (2–9). However, the predicted half-lives differ by many orders of magnitude; some half-lives approach the age of the Universe. This predicted island of stability sparked great interest in extending the periodic table out to the island by creating new elements in the laboratory and discovering them through searches in nature (10). More refined theoretical calculations (e.g., References 11–15) have been carried out. Although all approaches agree that at $N = 184$ there is a large spherical shell gap, different approaches provide $Z = 114$, 120, or 126 as the next spherical shell closure.

Also, refined calculations predicted large gaps in the single-particle energy levels for protons and neutrons at $Z = 102$ and 108 and $N = 152$ and 162 for deformed shapes. It is the reinforcements of these energy-level gaps at the same deformation that provide added stability and allow nuclei around these regions to have observable half-lives.

Two different experimental approaches, cold fusion and hot fusion, were used to extend the periodic table (for reviews, see References 16 and 17). The use of each approach required the construction of new separator facilities and the development of new detection methods designed to identify nuclei in newly discovered regions of SHN. Newly developed detection methods extended the range of measurable half-lives to lower limits of $\sim$1 μs. The cold fusion approach led to the discoveries of new elements with $Z = 107$–112, stabilized by reinforcing gaps between energy levels at deformation; the hot fusion approach led to the discoveries of new elements with $Z = 113$–118, nearer the island of stability of spherical nuclei (**Figure 2**).

2. HOW TO SYNTHESIZE SUPERHEAVY NUCLEI

2.1. Limitations of Using Light Projectiles

The fusion evaporation residue (EVR) cross section is determined by the product of the cross section for the formation of an SHN as a compound nucleus (CN) with excitation energy, E^*, multiplied by the probability of its survival, P_{xn} (E^*), during deexcitation by emission of x neutrons and γ-rays. The survival probability is proportional to the amount of neutron emission relative to fission, $\exp(-B_n)/\exp(-B_f)$, and therefore to an exponential function of $(B_f - B_n)$, the fission barrier height minus the binding energy of the neutron.

HILAC (the Heavy Ion Linear Accelerator) at LBNL (Lawrence Berkeley National Laboratory) and the 300-cm cyclotron at FLNR (Flerov Laboratory of Nuclear Reactions of the Joint Institute for Nuclear Research in Dubna, Russia) were the first accelerators to be used for searches for new elements. They could accelerate light ions only up to neon with sufficient intensity and energy for fusion reactions.

The more powerful 400-cm cyclotron U400 was built at FLNR, the linear accelerator Super-HILAC was constructed at LBNL, and UNILAC (the Universal Linear Accelerator) was built at GSI (Gesellschaft für Schwerionenforschung in Darmstadt, Germany) to provide wide ranges of projectiles for SHN production. Until approximately 1960, only hot fusion reactions were

Annu. Rev. Nucl. Part. Sci. 2013.63:383-405. Downloaded from www.annualreviews.org
Access provided by WIB6380 - Gesellschaft für Schwerionenforschung on 11/10/20. For personal use only.

Annu. Rev. Nucl. Part. Sci. 2013.63:383-405. Downloaded from www.annualreviews.org
Access provided by WIB6380 - Gesellschaft fur Schwerionenforschung on 11/10/20. For personal use only.

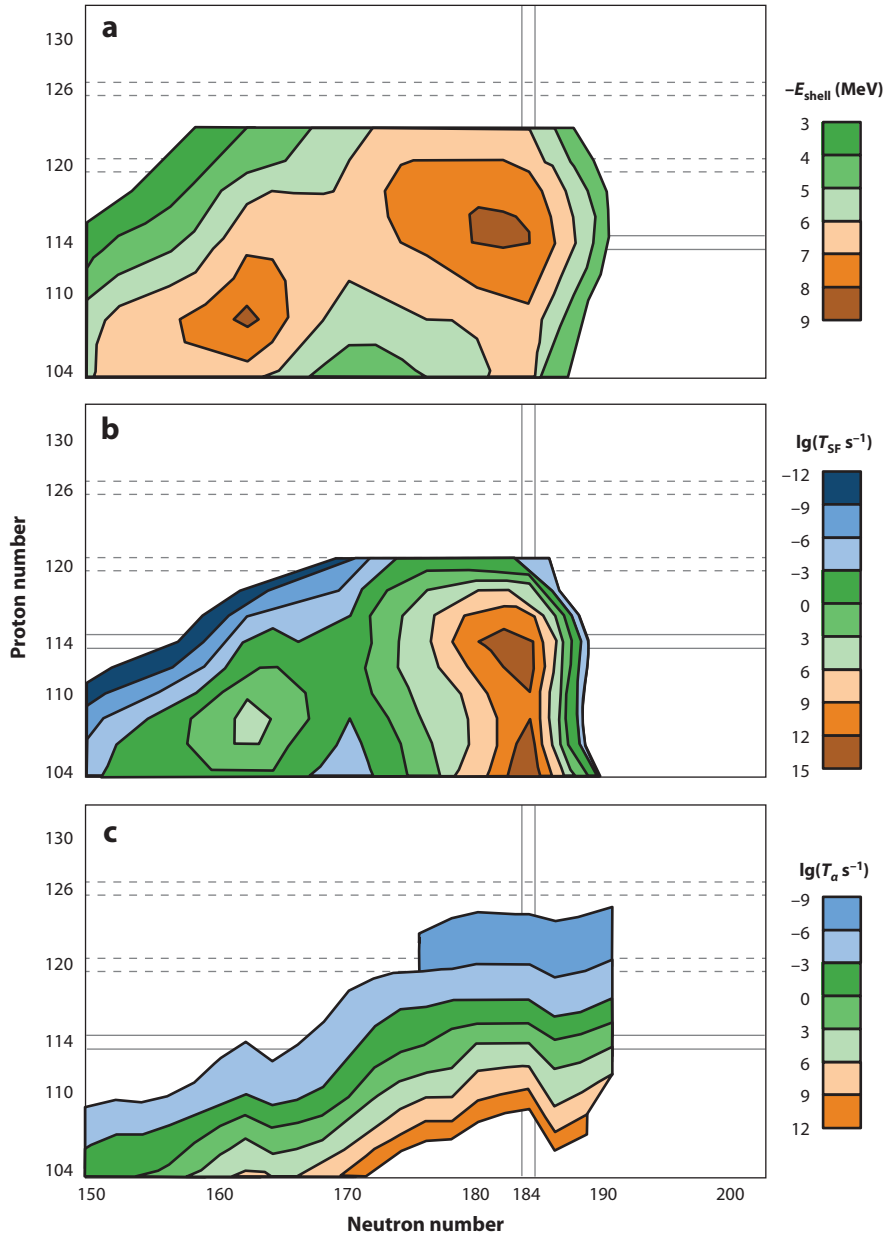

Figure 1

(*a*) Calculated ground-state shell-correction energy, (*b*) partial spontaneous fission (SF), and (*c*) α-particle half-lives (9).

studied because only light projectiles were available for acceleration. In hot fusion, the CN has high excitation energy, which causes the evaporation of three to five neutrons. In cold fusion, the CN has low excitation energy, so typically only one neutron evaporates. However, the use of lead or bismuth as the target demands heavier projectiles and more powerful accelerators to overcome the higher Coulomb barrier.

Annu. Rev. Nucl. Part. Sci. 2013.63:383-405. Downloaded from www.annualreviews.org
Access provided by WIB6380 - Gesellschaft fur Schwerionenforschung on 11/10/20. For personal use only.

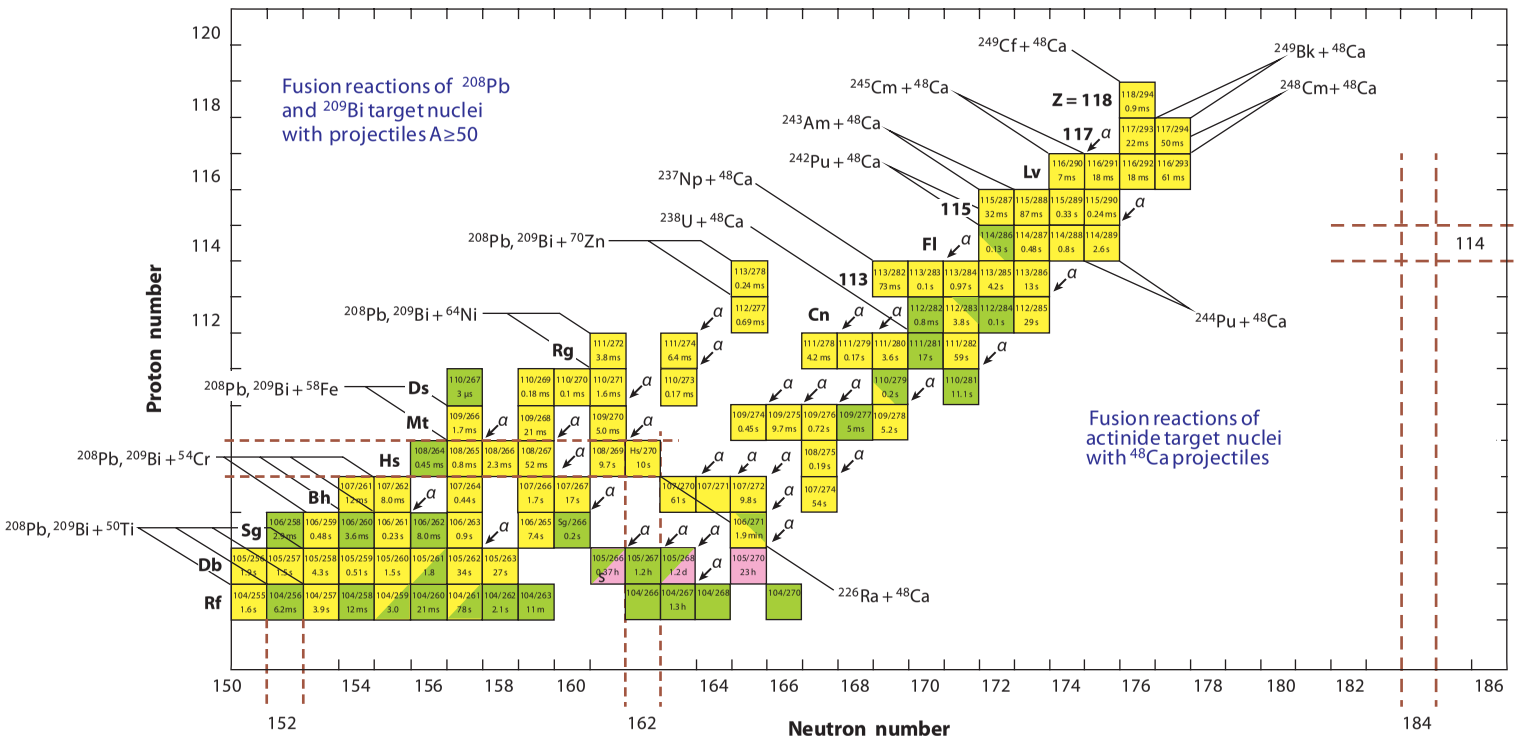

Figure 2

Most known nuclei (as of 2013) and the reactions required for their production. For each known isotope, the element name, mass number, and half-life are shown. The relatively neutron-deficient isotopes of the elements up to Z = 113 were created in cold fusion reactions. The more neutron-rich isotopes of elements 112–118 were produced in hot fusion reactions. Spherical closed shells for Z = 114 and N = 184 are shown. The bold dashed lines indicate nuclei with increased stability due to large gaps between the single-particle energy levels at Z = 108 and N = 152 and 162.

Annu. Rev. Nucl. Part. Sci. 2013.63:383-405. Downloaded from www.annualreviews.org
Access provided by WIB6380 - Gesellschaft fur Schwerionenforschung on 11/10/20. For personal use only.

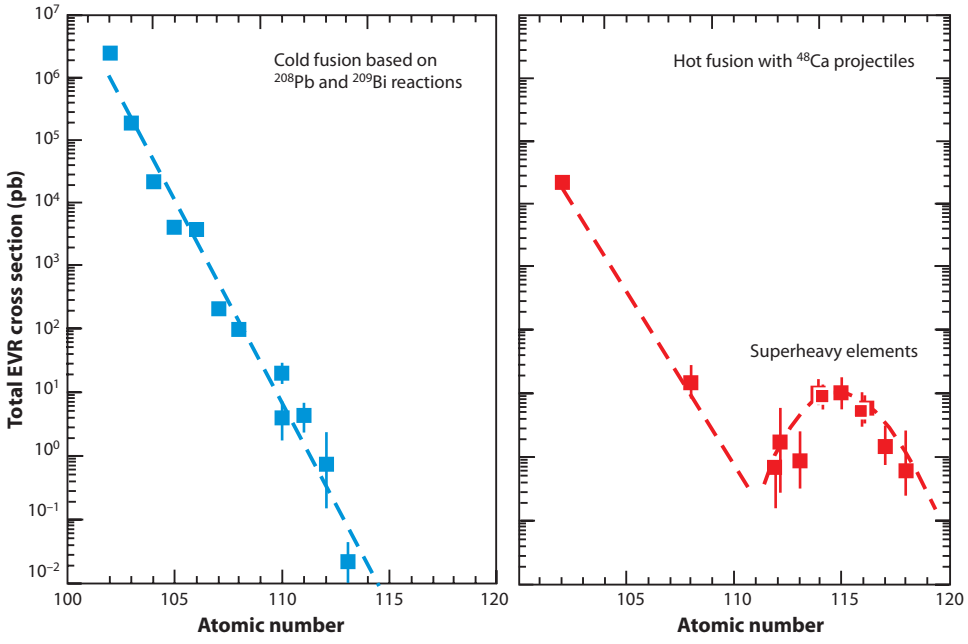

Figure 3

Measured cross sections for cold and hot fusion reactions. The total evaporation residue (EVR) cross section is the maximum value of the sum of neutron evaporation channels measured as a function of the beam energy.

2.2. The Cold Fusion Approach

The use of cold fusion to synthesize SHN was first considered at FLNR (18). In 1973, the detection methods were significantly improved, so the reaction $^{40}Ar + {}^{208}Pb \rightarrow {}^{248}Fm^{*}$ ($Z = 100$) yielded several hundreds to thousands of atoms in a single day (18, 19). The most significant result of this study was the relatively high probability of fusion of such massive nuclei. The largest cross sections were for the evaporation of two to three neutrons, providing convincing evidence that the use of doubly magic lead nuclei as target material could give rise to cold CN.

The cold fusion approach was successfully employed at GSI to discover the new elements 107–112. Exploiting cold fusion required not only a wide range of projectiles from UNILAC but also the development of a recoil separation technique, sensitive detector systems, fast electronic devices, and sophisticated analysis programs. SHIP (the Separator for Heavy Ion Reaction Products) was constructed at GSI for this purpose (20, 21). The rapidly decreasing cross section for the production of new, higher-Z elements in cold fusion (**Figure 3**) demanded the continuous development of ion sources to deliver higher currents. Also, cold fusion reactions between stable ^{208}Pb and ^{209}Bi and stable beams of ^{54}Cr and ^{70}Zn gave rise to EVRs that are shifted 10–15 mass units from the β-stability line to considerably decrease their half-lives.

2.3. The Hot Fusion Approach

Between element 102 and element 113, the cold fusion cross section decreases by a factor of approximately 10^8 (**Figure 3**). To reduce the contribution of factors that hinder fusion at higher

Z requires more asymmetric reactions (lower Coulomb barriers). To increase the neutron numbers of the EVRs to be closer to both the β-stability line and the new shell N = 184, both the target and projectile nuclei require maximum neutron excess. Long-lived, neutron-rich actinides such as ^{238}U, ^{244}Pu, ^{243}Am, ^{245}Cm, ^{248}Cm, ^{249}Bk, and ^{249}Cf have the greatest neutron excesses, so they can be used as target nuclei. The neutron-rich, doubly magic nucleus ^{48}Ca also has a clear advantage. For example, the CN ^{292}Fl produced in hot fusion of ^{244}Pu and ^{48}Ca acquires eight additional neutrons and has a 40%-lower Coulomb barrier compared with the cold fusion reaction of ^{208}Pb and ^{76}Ge. However, a CN produced in that fusion reaction would have an excitation energy of 30 to 40 MeV, which would lead to the evaporation of three to four neutrons. At each step, neutron emission and fission strongly compete with the survival probability, which depends (as mentioned above) on $\exp(B_f - B_n)$. Likewise, typical hot fusion reactions of actinide target nuclei with ^{22}Ne, ^{26}Mg, and ^{36}S projectiles to produce Z = 102–110 show a strong decrease in cross sections with an increase in Z_{CN} (**Figure 3**). This strong cross-section decrease is related to the decreasing nuclear survivability.

However, theoretical models that predicted the new closed shell at N = 184 also predicted strong shell effects for Z ≥ 112 and N ≥ 170 nuclei, which increase the fission barriers and raise their survivability. Therefore, hot fusion of actinide + ^{48}Ca nuclei offered the best opportunity to produce nuclei with Z > 112 and neutron numbers in the range of the predicted SHN island of stability. Indeed, the increase in the experimental cross sections for Z = 114–118 provides direct evidence of the existence and strong effect of a neutron shell located at N ≥ 180.

3. FACILITIES

The development of two different recoil separation techniques that use the ionic charge and momentum of the recoiling fusion products led to the discoveries of elements 107–112 by cold fusion and elements 113–118 by hot fusion.

3.1. UNILAC and the SHIP Velocity Filter

At GSI, UNILAC was coupled with the SHIP velocity filter. SHIP uses the kinematic properties of the fusion products, which differ from those of the projectile and other reaction products. High selectivity is achieved through the combination of electric and magnetic fields in the SHIP velocity filter (**Figure 4**). The detector station is the key to the identification of the transmitted EVRs and their decays, α emission, SF, or electron capture.

The present detector system is composed of three time-of-flight (TOF) detectors, eight identical 16-strip position-sensitive silicon detectors, and germanium detectors (22). **Figure 4** depicts the detector arrangement in the focal plane of SHIP. New isotopes are identified by their time and position correlation to known daughter decays. A TOF signal and an energy signal from the silicon detector provide the information needed to switch off the beam following detection of an implanted residue. After 20 μs, a time window of preset duration begins for counting a preset number of α particles. If the desired conditions are fulfilled, the beam-off period is prolonged to considerably reduce the background during the measuring period. Germanium detectors count γ-rays or X-rays in coincidence with signals from silicon detectors.

An alternative device that can be placed behind SHIP is a gas-filled stopping chamber coupled to a mass measurement trap (SHIPTRAP). By using SHIPTRAP, one can measure the masses of heavy nuclei with an accuracy of a few tens of keV (23).

Annu. Rev. Nucl. Part. Sci. 2013.63:383-405. Downloaded from www.annualreviews.org
Access provided by WIB6380 - Gesellschaft fur Schwerionenforschung on 11/10/20. For personal use only.

Annu. Rev. Nucl. Part. Sci. 2013.63:383-405. Downloaded from www.annualreviews.org
Access provided by WIB6380 - Gesellschaft fur Schwerionenforschung on 11/10/20. For personal use only.

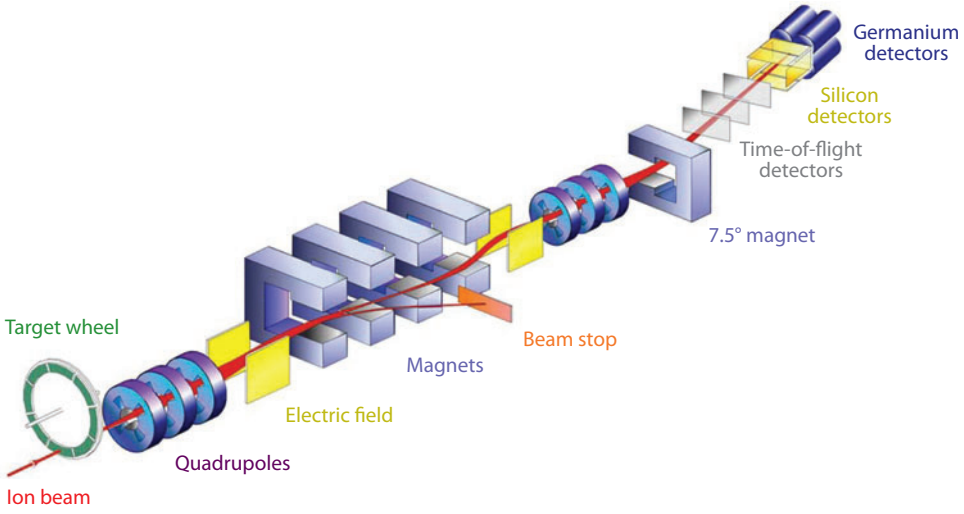

Figure 4

SHIP velocity filter and detectors at GSI.

3.2. The U400 Cyclotron and the Dubna Gas-Filled Recoil Separator

Another way to separate EVRs from all other reaction products is to use gas-filled separators. The functional concept of these devices is based on the different magnetic rigidities of the recoils and projectiles traveling through a low-pressure gas in a magnetic dipole field. The FLNR U400 cyclotron delivers a 1.2 p μA (1 p μA = 6.24 $\times 10^{12}$ particles s^{-1}) ^{48}Ca beam to the rotating target of DGFRS (the Dubna gas-filled recoil separator) (**Figure 5**) (17). The large dipole magnet chamber is filled with hydrogen gas. The transit time for the EVRs is ∼1 μs; the transmission efficiencies are ∼35–40%.

EVRs passing through the separator are implanted in a 4 × 12 cm^2 silicon detector with 12 vertical position-sensitive strips. To detect escaping α particles, the front detector is surrounded by eight 4 × 4 cm^2 side detectors. The position-averaged detection efficiency for full-energy α particles of implanted nuclei is 87% of 4π.

Before implantation, the separated EVRs pass through a TOF system that shows that a nucleus came from the separator. During target irradiation, the beam is switched off after a recoil signal with preselected energy and TOF is detected; subsequently, an α particle–like signal with preselected energy and decay time is detected.

Other gas-filled separators, such as BGS at LBNL; the separator at IMP in Lanzhou, China; GARIS at RIKEN, Japan; and TASCA at GSI differ in, for example, their magnetic systems, deflecting angle, use of helium gas instead of hydrogen, and focal plane detector array. However, they use the same principle of operation, and their characteristics of SHN transmission and separation power are similar (24–28).

4. COLD FUSION REACTIONS

4.1. Cold Fusion Studies at GSI with SHIP

In addition to helping ensure the success of the FLNR cold fusion experiments, technical considerations were crucial for the choice of cold fusion experiments at SHIP. Targets of stable lead and

Annu. Rev. Nucl. Part. Sci. 2013.63:383-405. Downloaded from www.annualreviews.org
Access provided by WIB6380 - Gesellschaft fur Schwerionenforschung on 11/10/20. For personal use only.

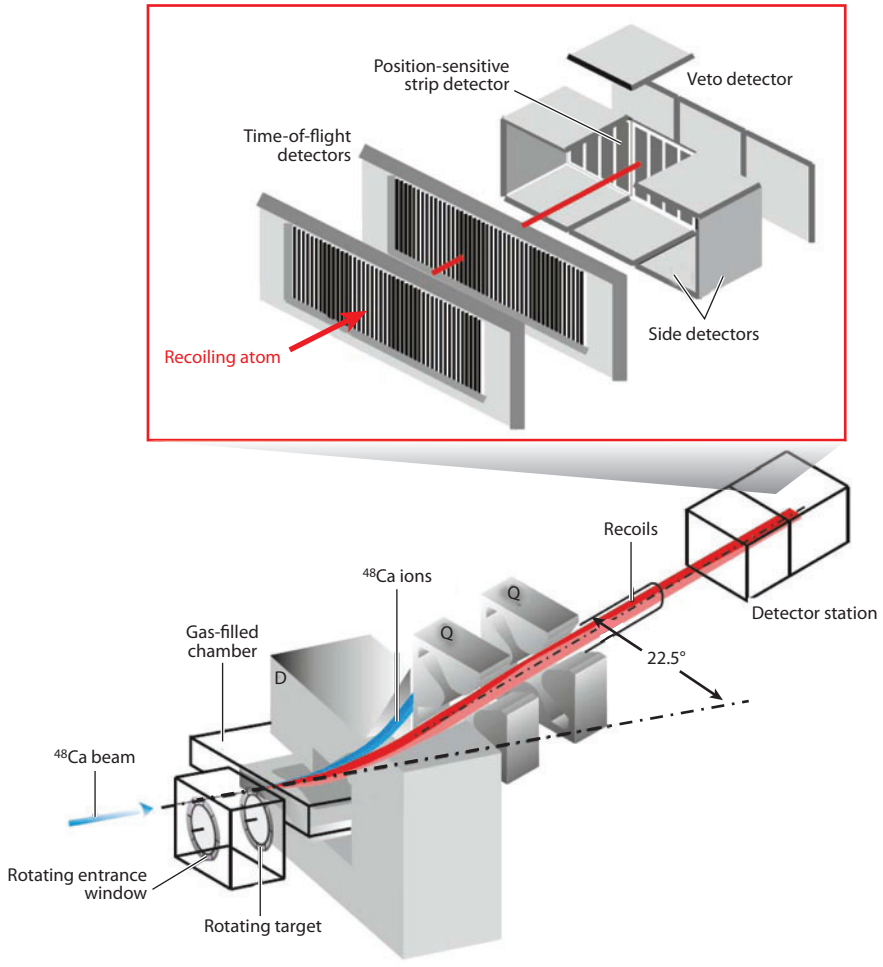

Figure 5

The Dubna gas-filled recoil separator and detectors.

bismuth isotopes are inexpensive and easy to handle. Furthermore, with beams of ^{40}Ar or heavier elements, the velocities of EVRs are much higher than they are in typical hot fusion experiments, which use heavier targets and lighter projectiles. At higher velocities, and with the evaporation of only one neutron, the separator efficiency increases. SHIP transmission has reached values of 40% to 60%.

In initial SHIP experiments, physicists studied the cold fusion reaction $^{40}\mathrm{Ar} + {}^{208}\mathrm{Pb} \rightarrow {}^{246}\mathrm{Fm} + 2n$, and earlier results obtained at FLNR were confirmed. The search for element 107 was initiated through studies of its expected daughter nucleus, produced in the reaction $^{50}\mathrm{Ti} + {}^{209}\mathrm{Bi} \rightarrow {}^{258}105 + 1n$. **Figure 2** summarizes the reactions and decay chains measured in cold fusion.

4.2. Discoveries of the New Elements 107–112 at GSI

The discoveries of elements 107–112 in cold fusion reactions at GSI are described below in chronological order. We also discuss cross-bombardment verifications and more recent confirmations at other laboratories.

Annu. Rev. Nucl. Part. Sci. 2013.63:383-405. Downloaded from www.annualreviews.org
Access provided by WIB6380 - Gesellschaft fur Schwerionenforschung on 11/10/20. For personal use only.

4.2.1. Element 107, bohrium. Following the success of the first two cold fusion reactions, the search began for bohrium (Z = 107), the first new element to be synthesized at SHIP. Investigators used the reaction $^{54}Cr + {}^{209}Bi \rightarrow {}^{263}Bh^* \rightarrow {}^{262}Bh + 1n$. In 1981, five decay chains of ^{262}Bh were observed (29). The subsequent decay chain from $^{258}105$ is consistent with the $^{258}105$ chain observed in the $^{209}Bi + {}^{50}Ti$ reaction. This cross-bombardment verification is an important confirmation of the identification of a new element. The isotope ^{261}Bh was later synthesized at a higher beam energy (30). The new isotopes ^{265}Bh and $^{266,267}Bh$ were produced in hot fusion reactions at IMP in Lanzhou (27) and at LBNL (31, 32), respectively.

4.2.2. Element 109, meitnerium. The next new element, meitnerium (Z = 109), was synthesized in 1982. In the reaction $^{58}Fe + {}^{209}Bi$, a single α-decay chain of ^{266}Mt was observed (33); this isotope α-decayed to the previously observed ^{262}Bh. The observation of this chain accorded with the previously observed daughter nucleus, $^{262}107$. Again, this discovery was verified by cross-bombardment results. Subsequently, more events were observed at GSI (34, 35) and LBNL (36).

4.2.3. Element 108, hassium. The next new element to be discovered was hassium (Z = 108), which was synthesized in 1984 by use of the reaction $^{58}Fe + {}^{208}Pb$. This experiment was preceded by a study of hassium's daughter nucleus, $^{261}106$, in the reaction $^{54}Cr + {}^{208}Pb$. Three events of $^{265}108$ were observed (37), and with a target of ^{207}Pb, one event was assigned to $^{264}108$ (38); both observations were later confirmed (39). Subsequently, the isotopes ^{269}Hs, ^{270}Hs, and ^{271}Hs were discovered in the hot fusion reaction $^{26}Mg + {}^{248}Cm$ in the $5n$, $4n$, and $3n$ channels, respectively (40). The decay properties of ^{270}Hs, located in the center of deformed nuclei (**Figure 1**), were studied and synthesized in the reactions $^{248}Cm + {}^{26}Mg$ (41) and $^{226}Ra + {}^{48}Ca$ (42). In these experiments, physicists detected six identical α-SF decay chains of the nucleus ^{270}Hs that corresponded to a cross section of $\sigma_{4n} = 16^{+12}_{-7}$ pb. The partial α-decay half-life of ^{270}Hs was measured for the first time; the result was $T_\alpha = 7.6^{+4.9}_{-2.2}$ s. The decay properties of ^{270}Hs corroborate theoretical predictions of its relatively high stability, which arises from the effect of large single-particle energy gaps at Z = 108 and N = 162.

4.2.4. Element 110, darmstadtium. Darmstadtium (Z = 110) was discovered in 1994 in the reaction $^{62}Ni + {}^{208}Pb \rightarrow {}^{269}Ds + 1n$ (39). This experiment was preceded by a study that obtained accurate results of the excitation functions for the synthesis of ^{257}Rf and ^{265}Hs. The data revealed that the maximum cross section for the synthesis of element 108 was shifted to a lower excitation energy relative to that for element 104; this observation differed from theoretical reaction predictions. The isotope ^{271}Ds was synthesized with a more neutron-rich ^{64}Ni beam (43). The fact that the cross section was enhanced from 2.6 to 15 pb by use of a projectile with two additional neutrons led experimenters to hope that the synthesis of heavier elements would decrease less steeply. However, this was not the case for element 112.

The 13 decay chains observed for ^{271}Ds yielded two half-lives of ~1.8 and 65 ms. A decade later, these results were confirmed at RIKEN (26) with 14 decay chains observed in the same reaction. Obviously, isomeric states are involved. Because the measured α-particle energies are almost identical, the likely explanation is that the isomeric state has a longer half-life and decays by γ-rays or conversion electrons to the ground state. Furthermore, the appearance of ^{271}Ds in the same reaction was confirmed for three beam energies at BGS (44) and for one beam energy at IMP in Lanzhou (45). The ^{267}Ds observed by LBNL in cold fusion reactions and the ^{273}Ds observed by FLNR in hot fusion reactions require further experimental clarification.

The even–even nucleus ^{270}Ds was synthesized in the reaction ^{64}Ni + ^{207}Pb (46) with 8 events and, subsequently, 25 additional events. The data were obtained for the ground state and a longer-lived (6.0-ms) high-spin *K* isomer.

4.2.5. Element 111, roentgenium. Roentgenium (Z = 111) was synthesized in 1994 by use of the reaction ^{64}Ni + ^{209}Bi → ^{273}Rg*. Three α-chains were observed (47), and another three were reported in a confirmation experiment. The GSI data on ^{272}Rg were confirmed at RIKEN when 14 chains were observed (48). In one case, the chain terminated by SF after population of ^{260}Db, and in two cases, the chain terminated by SF after population of ^{264}Bh. Whether the two nuclei decayed by SF or by electron capture (EC) to ^{260}Rf and ^{264}Sg, which are known SF nuclei, is unknown. The appearance of ^{272}Rg was reconfirmed at LBNL (49).

4.2.6. Element 112, copernicium. Copernicium (Z = 112) was first observed in 1996 at SHIP through the reaction ^{70}Zn + ^{208}Pb → ^{278}112* (50). In this experiment, one chain was observed. A second chain was observed in a separate experiment in 2000 (51). In 2004, the ^{70}Zn + ^{208}Pb → ^{278}112* reaction was repeated at RIKEN (52), and the observation of two more decay chains, including the SF branch of ^{261}Rf, confirmed the discovery of this element.

4.3. Production of ^{278}113 at RIKEN

The ^{278}113 isotope was investigated at GSI in 1998 in the reaction ^{70}Zn + ^{209}Bi → ^{279}113* with a beam dose of 7.5 × 10^{18} (22) and in 2003 with a dose of 7.4 × 10^{18} (53). The combination of these two SHIP experiments yielded an upper one-event cross-section limit of 160 fb. A similar search experiment was initiated at RIKEN in 2003–2004. With a beam dose of 17 × 10^{18}, one decay chain was observed and assigned to ^{278}113 (54) with $\sigma = 55^{+150}_{-45}$ fb. The lower cross section reached was made possible by the higher efficiency of 80% (instead of 50%) and the thicker target at RIKEN. This experiment was continued in 2005–2006 and yielded a second event that agreed with the first (55). The experiment was continued off and on between 2008 and August 2012, when a third chain was observed. The total beam time was 553 days, and $\sigma(113) = 22^{+20}_{-13}$ fb (56). The three events agree through ^{262}Db, in which the third event continued with two more α decays to ^{254}Md to establish the identification of the isotope ^{278}113.

Attempts to synthesize heavier elements with cold fusion reactions were unsuccessful. See Reference 16 for a review.

4.4. Direct Mass Measurements with Ion Traps

A basic property of nuclei is their binding energy. The binding energy is manifested by the nuclear mass, which characteristically differs from the sum of the masses of the constituent protons and neutrons. By taking advantage of the techniques developed for the production of rare nuclei in experiments at high beam intensities, the Penning trap system SHIPTRAP, mounted behind SHIP at GSI, has explored mass measurements of nuclei in the region of the heaviest nuclei. So far, SHIPTRAP has measured the masses of the nuclei $^{252–255}$No and ^{255,256}Lr; five of these measurements had an accuracy of ~15 keV (23, 57).

The nuclei were produced in reactions between a ^{48}Ca beam and targets of $^{206–208}$Pb and ^{209}Bi. The mass measurement of ^{256}Lr ($T_{1/2}$ = 27 s) was challenging to perform; this isotope was produced with a cross section of only 60 nb. During a measuring time of 93 h, a mass value was determined from 48 detected ions that had an accuracy of 83 keV.

Annu. Rev. Nucl. Part. Sci. 2013.63:383-405. Downloaded from www.annualreviews.org
Access provided by WIB6380 - Gesellschaft fur Schwerionenforschung on 11/10/20. For personal use only.

The new masses are used as anchor points for determining the masses of both lighter and heavier nuclei by use of measured α-decay Q values of decay chains. Thus, the mass of ^{270}Ds has been experimentally established with an accuracy of 40 keV. This mass is the heaviest anchor point in the region of the large single-particle energy gaps at Z = 108 and N = 162.

5. HOT FUSION REACTIONS

5.1. Hot Fusion Studies at FLNR

Because of the need to synthesize nuclei with high numbers of neutrons so as to reach higher Z than in cold fusion, FLNR pioneered reactions between actinide targets and neutron-rich ^{48}Ca that led to the discovery of new elements 113–118. FLNR had to solve the problem of the optimum beam energies for the deformed actinides and determine how to identify the isotopes produced, given that their total decays were in an unknown region.

Beginning in 1998, DGFRS used fusion reactions between ^{48}Ca and targets made from enriched isotopes of radium, uranium, neptunium, plutonium, americium, curium, berkelium, and californium (11 isotopes of 8 elements) (17). In 2003, FLNR measured excitation functions for reactions with ^{242,244}Pu, yielding consistent interpretations of previously observed reactions. **Figure 2** shows the hot fusion reactions and decay chains measured at FLNR. Also shown in this figure are the data obtained at LBNL and at GSI.

5.2. Discoveries of New Elements 113–118 at FLNR

The discoveries of elements 113–118 in hot fusion reactions at FLNR are described below in chronological order. For elements 113, 115, 117, and 118, we present recent definitive evidence for their discoveries, including many new events, cross-bombardment verifications, and confirmations at other laboratories.

5.2.1. Element 114, flerovium. Flerovium (Z = 114) was discovered in the hot fusion reactions ^{242,244}Pu + ^{48}Ca (58–62). In the reaction ^{242}Pu + ^{48}Ca, performed at four different energies, 1 2*n*, 15 3*n*, and 9 4*n* decay chains that corresponded to ^{288}114, ^{287}114, and ^{286}114, respectively (58), were observed. In later ^{244}Pu + ^{48}Ca reaction studies performed at five energies, 1 5*n*, 12 4*n*, and 5 3*n* chains corresponding to ^{287}114, ^{288}114, and ^{289}114, respectively, were observed (59, 60). Cross-bombardment verification was obtained from the decay of element 116 (discussed in the following section) and from the 3*n* and 4*n* reactions of ^{238}U + ^{48}Ca, in which the same isotopes, ^{283,282}112 (58), the daughter nuclei of ^{287,286}114, were observed. The agreement between the decay properties of the isotope ^{283}112 observed in these three reactions is very good (**Figure 2**). In the ^{285}112 decays, two α energies ($\sim$0.2 MeV and $\sim$0.6 MeV below the main E_α) were observed, indicating that the first two excited states of ^{281}110 were populated.

Subsequently, researchers at GSI used TASCA to study the reaction ^{244}Pu (^{48}Ca, 3*n*–4*n*) ^{289,288}114 so as to confirm the discovery of element 114. The results agreed well with those from the previously observed decay chains (28). A previously unobserved α branch in ^{281}Ds was observed to populate the new nucleus, ^{277}Hs, which then decayed by SF. The cross-section data (28) obtained from TASCA fully confirmed the large cross sections reported for SHN production at DGFRS.

At BGS, the reaction ^{242}Pu (^{48}Ca, 5*n*) was used to observe one decay chain of the new isotope ^{285}114, which underwent five α decays before ^{265}Rf underwent SF (25). The properties of a second decay chain, one α decay followed by SF, agreed with those previously assigned to ^{286}114.

Annu. Rev. Nucl. Part. Sci. 2013.63:383-405. Downloaded from www.annualreviews.org
Access provided by WIB6380 - Gesellschaft fur Schwerionenforschung on 11/10/20. For personal use only.

5.2.2. Element 116, livermorium. The reaction ^{248}Cm + ^{48}Ca was used to synthesize two isotopes ^{293}116 (3*n*) and ^{292}116 (4*n*) (58, 63). These isotopes underwent R − α_1 − α_2 − α_3 − SF and R − α_1 − α_2 − SF decays, which had lifetimes of 89 and 26 ms, respectively. For both isotopes, the first α decays populated ^{289,288}114, which were observed in the ^{244}Pu (^{48}Ca, 3*n*–4*n*) ^{289,288}114 reactions (**Figure 2**). The good agreement between the ^{289,288}114 decays populated in these two reactions provided two cross-bombardment verifications of the discoveries of elements 116 and 114. In one case, the 9.48-MeV ^{289}114 α-decay energy differed from that determined from nine other sequences (9.82 MeV), probably indicating a transition to an excited state.

The ^{245}Cm + ^{48}Ca reaction was studied at several beam energies, wherein 15 correlated decay chains of two types—R − α_1 − α_2 − SF with a total decay time of 10 s and R − α_1 − (α_1/SF) − SF with a decay time of 0.5 to 0.9 s—were observed (60, 65). Again, there is good agreement between the decay properties for ^{287}114 and ^{286}114 populated in the ^{245}Cm and ^{242}Pu reactions where there is overlap. These decay properties provide additional cross-bombardment verification of 116 and 114.

The reaction ^{238}U (^{48}Ca, 3*n*–4*n*) ^{283,282}112 was studied at three energies. Seven events were observed for ^{283}112 and one for ^{282}112 (58). Together, these eight chains agreed with the chains of the daughter nuclei of ^{287,286}114, and of the grand-daughter nuclei of ^{291,290}116, providing further independent verification of elements 114 and 116.

The reaction ^{48}Ca + ^{238}U → ^{283}112 + 3*n* was studied at SHIP at three beam energies in 2005–2007. The results confirmed the FLNR data. Two R − SF and two R − α − SF events were observed. The R − SF events were assigned to a 50% branch of ^{283}112. The FLNR data on element 116 were also confirmed at SHIP by use of the reaction ^{48}Ca + ^{248}Cm → ^{296}116* (66). Four decay chains agreed with the decay of ^{292}116 (4*n*) and one with ^{293}116 (3*n*), observed previously.

5.2.3. Element 118. At DGFRS, the reaction ^{249}Cf + ^{48}Ca was studied at two beam energies (67, 68). With a beam dose of 2.5 × 10^{19} at $E^* = 29.2$ MeV and a target that was 0.23 mg cm^{-2} thick, one R − α_1 − α_2 − SF decay chain that lasted 0.56 s was observed (60). In a second experiment conducted in 2005, with a beam dose of 1.6 × 10^{19}, $E^* \approx 34.4$ MeV, and a target that was 0.34 mg cm^{-2} thick, two additional events were observed: R − α_1 − α_2 − SF and R − α_1 − α_2 − α_3 − SF (68). For these three events, the first two α energies agree. The agreement between energy and decay time shows that all three belong to the same nucleus. A comparison between these decay chains and those of ^{291,290}116, produced in the ^{245}Cm + ^{48}Ca reaction, yielded agreement for ^{290}116. Thus, the new isotope is ^{294}118.

In a recent ^{249}Bk + ^{48}Ca experiment in which ^{249}Cf from the β decay of ^{249}Bk was in the target after long irradiation, one additional chain of ^{294}118 was observed. Its decay properties agreed with those observed in the three earlier events (69).

5.2.4. Elements 113 and 115. Elements 113 and 115 were synthesized for the first time in 2003 by use of the reaction ^{243}Am + ^{48}Ca with 248 MeV ^{48}Ca ($E^* \approx 40$ MeV) and a beam dose of 4.3 × 10^{18} (70, 71). Three R − α_1 − α_2 − α_3 − α_4 − α_5 − SF events were observed. All the α particles were detected in a total time of 15 to 29 s, and SF occurred between 17 and 29 h after the last α decay. These three events were assigned to the decay of the isotope ^{288}115 produced in the 3*n* evaporation channel. This isotope decayed to the previously unknown isotope ^{284}113. At $E^* \approx 44.5$ MeV and a beam dose of 4.3 × 10^{18}, such decays were not observed. However, at this excitation energy, one other event with five α decays (the fifth α particle was not detected) and

Annu. Rev. Nucl. Part. Sci. 2013.63:383-405. Downloaded from www.annualreviews.org
Access provided by WIB6380 - Gesellschaft fur Schwerionenforschung on 11/10/20. For personal use only.

SF was measured; this event has been assigned to the decay of the neighboring isotope $^{287}115$, a product of the 4*n* evaporation channel.

To definitively establish the discoveries of elements 113 and 115, experiments reinvestigated the reaction $^{243}Am + {}^{48}Ca$ at DGFRS at five energies in 2011–2012 (72–74). Twenty-eight new $^{288}115$ decay chains were observed along with one new $^{287}115$ chain; these observations agreed completely with the earlier $^{288,287}115$ data. The total of 31 $^{288}115$ and $^{284}113$ events represents clear evidence of the discoveries of elements 113 and 115. At the lowest bombarding energy, four new decay chains ($R - \alpha_1 - \alpha_2 - SF$) were observed and were assigned to $^{289}115$ (**Figure 2**). The $^{289}115$ chains are the same as those observed following the α decay of $^{293}117$ to $^{289}115$, which in turn α-decays to $^{285}113$. The agreement between these four new events and the $^{293}117$ data provide definitive cross-bombardment evidence for the discoveries of elements 113, 115, and 117.

5.2.5. Element 117. A new collaboration including researchers at Oak Ridge National Laboratory and Vanderbilt University obtained a source of ^{249}Bk ($T_{1/2} = 320$ days) from the Oak Ridge HFIR (High-Flux Isotope Reactor). At DGFRS, studies of the reaction $^{249}Bk + {}^{48}Ca$ at beam energies of 252 and 247 MeV and beam doses of 2.4×10^{19} and 2.0×10^{19} led to the discovery of element 117 (75, 76). At the higher energy, five events were observed with three α particles and SF; they were assigned to the decay of $^{293}117$ (4*n* evaporation channel). At the lower energy, one chain was observed with five α particles and SF; it was assigned to the decay of $^{294}117$. Both the odd proton and the odd neutron hindered SF, allowing the chain to continue. The $^{289}115$ decays that were populated in the ^{245}Am and ^{249}Bk reactions provided definitive cross-bombardment verification for the discoveries of elements 113, 115, and 117 (**Figure 2**).

In 2012, a second ^{249}Bk source was obtained, and the experiment was repeated at two energies corresponding to the 3*n* and 4*n* cross-section maxima. Two $^{294}117$ events and five $^{293}117$ events were observed (69). The experiment was continued, yielding one additional $^{294}117$ event and six additional $^{293}117$ events. All their decay properties agreed with those from the earlier results (75, 76). The buildup of ^{249}Cf from the ^{249}Bk β decay enabled the observation of one $^{294}118$ event (69).

The 2012 ^{249}Bk material was divided between Dubna and GSI. The search for element 119 is discussed below. In a further confirmation of the discovery of element 117, a $^{249}Bk + {}^{48}Ca$ run at TASCA observed the 4*n* evaporation channel $^{293}117$ isotope (77).

5.3. Chemical Experiments

Observations of the chemical behavior of the new atoms were important in establishing the position of these nuclei in the periodic table of the elements and in independently confirming the Z of isotopes produced in hot fusion actinide + ^{48}Ca reactions. The first chemical experiment involved ^{268}Db ($T_{1/2} \approx 1.2$ days), which should belong to group five of the periodic table as a heavier homolog of tantalum. The reaction used was $^{243}Am + {}^{48}Ca \rightarrow {}^{288}115 + 3n$. Because all consecutive α decays and SF are strongly correlated and their order determined, the identification of the atomic number of any nucleus in this chain independently proves the synthesis of the previously unknown elements 115 and 113. In the first experiment, all 15 SF events corresponded to the decay of the group-five nuclide, Z = 105 (61, 78).

In a second, more sophisticated experiment, the group-five elements (niobium, tantalum, and dubnium) were separated from those of group four (zirconium, hafnium, rutherfordium), and the homologs niobium and tantalum were separated (62). Five events corresponding to the decay of ^{268}Db were observed in the group-five fraction; these observations support the relationship between ^{268}Db and its homolog, tantalum. These two experiments, each with 20 events

Annu. Rev. Nucl. Part. Sci. 2013.63:383-405. Downloaded from www.annualreviews.org
Access provided by WIB6380 - Gesellschaft fur Schwerionenforschung on 11/10/20. For personal use only.

(61, 62, 78), definitively established that Z = 115 for the initial EVR and thus independently confirmed the discoveries of elements 115 and 113.

As a consequence of the considerable increase in the half-lives of the elements produced in ^{48}Ca-induced reactions, one can study their chemical behavior. It has now become possible to check the similarities or differences between the chemical properties of the heaviest elements and those of their light homologs.

Among synthesized SHN, those that are most suitable for this purpose are the isotopes ^{283}112, ^{285}112, ^{285}113, and ^{286}113 that undergo α-SF decay. To what extent element 112 (for example) is a homolog of mercury depends on the so-called relativistic effect in the electronic structure of the superheavy atom. Will element 112 interact as actively as mercury does with gold (79, 80) or—exactly the opposite—will it be closer to the chemically neutral radon (81)? The reaction $^{242}\mathrm{Pu} + {}^{48}\mathrm{Ca} \rightarrow {}^{287}114 + 3n$ ($T_{1/2} \approx 0.5$ s) was used to produce the isotope ^{283}112 ($T_{1/2} \approx 4$ s) via α decay.

Both characteristics—high volatility and the ability to form intermetallic compounds for mercury, radon, and element 112 atoms—defined the experimental setup for the chemical identification of element 112 (82). The recoil nuclei leaving the ^{242}Pu target stopped in a helium/argon-gas medium. Only high-volatility nuclei were transported to the detectors. The transport time from the stopping chamber to the detectors was 3.6 s. In three experiments, performed at different transport velocities of the recoil nuclei, five atoms of the isotope ^{283}112 undergoing sequential α-SF decay were detected; their characteristics completely coincided with those from previous observations at the gas-filled separator.

For element 112 atoms, as well as for mercury atoms, experimenters have observed adsorption on the gold surface of the detectors (83). This observation is evidence of the formation of an intermetallic compound [112 · Au]. Moreover, the distribution of the adsorbed atoms with Z = 112 as a function of temperature is shifted relative to mercury in the direction of lower temperatures, indicating the high volatility of element 112. Herein lies the difference between the properties of mercury and those of element 112, which can be explained by relativistic calculations (80). FLNR is currently performing experiments with atoms of elements 113 and 114.

6. RESULTS AND WHAT WE HAVE LEARNED

In this section, we discuss the stability of SHN as observed in their lifetimes, decay modes, and production cross sections, as well as how they vary as a function of Z and N. We also describe their proximity to the region of increased stability of deformed nuclei at Z = 108 and N = 162 and the predicted spherical closed shells at Z = 114, 120, or 126 and N = 184.

6.1. α Decay

Nearly all the new elements for Z = 107–112 produced in cold fusion undergo a chain of α decays followed by SF or, in a few cases, by EC and SF. Sometimes SF occurs without a preceding α decay; for example, ^{264}Hs produced in the reaction $^{207}\mathrm{Pb} + {}^{58}\mathrm{Fe}$ (1n) has a 50% SF branch. These α chains end in the SF of known isotopes to firmly establish the initial Z. Similarly, in hot fusion the new elements Z = 113–118 undergo an α-decay chain followed by SF.

Figure 6*a* compares the experimental and theoretical α-decay energies of nuclides with Z = 106–118, synthesized in cold fusion with Pb and Bi targets, and **Figure 6*b*** compares these values in actinide + ^{48}Ca hot fusion reactions. The hot and cold fusion values in $\Delta Q_\alpha = Q_\alpha(\mathrm{exp.}) - Q_\alpha(\mathrm{theor.})$ for calculations performed in a macroscopic-microscopic model (9, 84, 85) show that, for all even-Z nuclei with Z = 106–118 and A = 260–294 and for odd-N nuclei, ΔQ_α does not

Annu. Rev. Nucl. Part. Sci. 2013.63:383-405. Downloaded from www.annualreviews.org
Access provided by WIB6380 - Gesellschaft fur Schwerionenforschung on 11/10/20. For personal use only.

Annu. Rev. Nucl. Part. Sci. 2013.63:383-405. Downloaded from www.annualreviews.org
Access provided by WIB6380 - Gesellschaft fur Schwerionenforschung on 11/10/20. For personal use only.

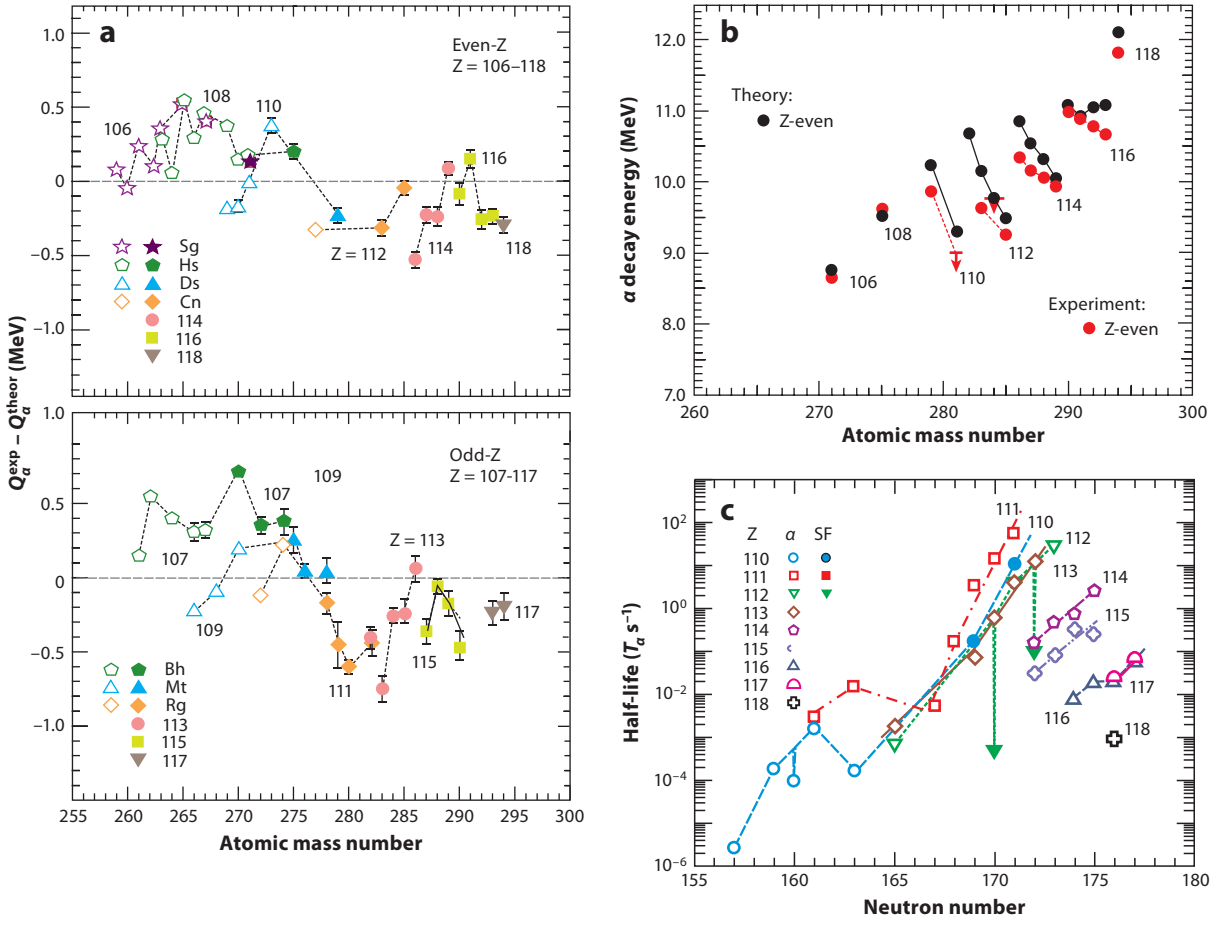

Figure 6

(*a*) Differences in measured α-decay energies, Q_α(exp.) and Q_α(theor.), calculated with a macroscopic-microscopic model (9). Filled symbols represent nuclei synthesized in hot fusion reactions; open symbols represent those synthesized in cold fusion reactions. (*b*) For hot fusion reactions, the actual experimental and theoretical α-decay energies. (*c*) The α half-lives for hot ($N > 166$) and cold ($N < 166$) fusion as a function of neutron number. The 111, $N = 170$ is for SF. Abbreviation: SF, spontaneous fission.

exceed 0.5 MeV; these data also show that for odd-Z nuclei, $\Delta Q_\alpha \leq 1.0$ MeV. **Figure 6*c*** shows the T_α half-lives for hot and cold fusion. Approaching N = 184 should decrease Q_α and increase T_α, as has been experimentally demonstrated even for nuclei with Z ≥ 110 and 10–12 neutrons removed from 184. These findings lend strong support for the island-of-stability hypothesis. The theoretical predicted shell closure at N = 184 is supported by the steep rise in T_α as N increases from 171 to 174 for elements 114 and 115 (**Figure 6*c***).

Calculations of SF and α half-lives for Z = 100–126 were recently performed in the Hartree–Fock–Bogoliubov approach by use of the finite-range, density-dependent Gogny force with the deep-inelastic scattering parameter set (86). The authors of this study find very good agreement between experimental $T_{1/2}(\alpha)$ and their calculations for cold fusion data with N ≤ 162 and hot fusion data for Z = 114, 116, and 118. They note that the local maxima found in all elements in the partial α and SF half-lives at N = 162 arise from the special character and stability associated with

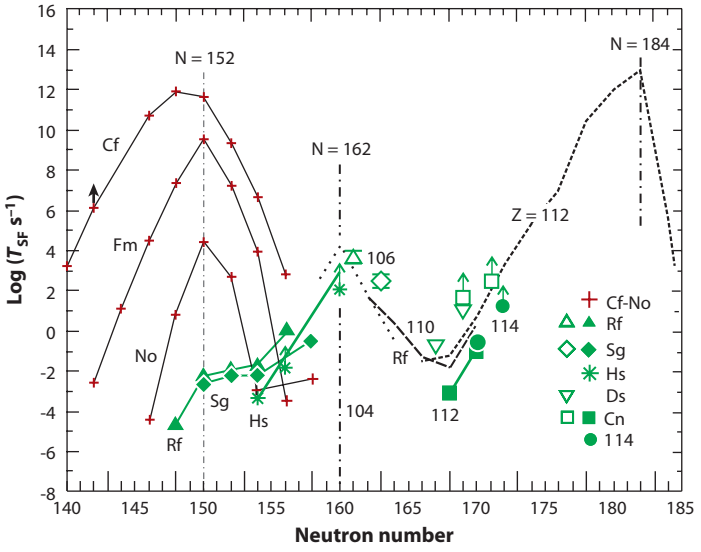

Figure 7

Spontaneous fission half-lives versus N. The solid symbols and crosses denote even–even nuclei; open symbols denote even–odd nuclei. Solid lines are drawn through the experimental points of even–even nuclei. The dashed lines represent theoretical calculations of T_{SF} (9). Abbreviation: SF, spontaneous fission.

N = 162. This finding is related to the large gap between single-particle energy levels at N = 162 for deformed nuclei, which provides added stability. Therefore, both the macroscopic-microscopic and Hartree–Fock–Bogoliubov approaches found overall agreement with the experimental results.

6.2. Spontaneous Fission

Of the 47 nuclei synthesized in hot fusion, 11 decay predominantly via SF; for 2 others, SF and α decay compete. **Figure 7** shows the partial SF half-lives, T_{SF} versus N, for even-Z nuclei with Z = 98–114. Note that for N $\geq$ 170, the partial SF half-lives rise steeply, so two additional neutrons in ^{284}112, compared with ^{282}112, increase T_{SF} by two orders of magnitude (**Figure 7**). A similar effect is observed for ^{286,288}114. This increase is related to the increase in neutron number toward the N = 184 spherical shell closure. The odd-A isotopes ^{183,185}112 undergo α decay. The odd neutron imposes a hindrance to SF $\geq 10^3$.

For nuclei with Z < 110 and N < 170, T_{SF} increases again when N = 162 is approached, as shown in **Figure 7** for rutherfordium, seaborgium, and hassium. Below N = 162, the SF half-lives decrease. There exists a sharp maximum in T_{SF} at N = 162, providing strong support for the presence of increased stability due to the large gap between single-particle energy levels at N = 162. For the same reason, an even more pronounced peak in partial fission half-lives is observed at N = 152.

Aided by the hindrance of the odd proton, odd-Z isotopes with Z > 111 and N $\geq$ 172 that are produced in reactions of ^{48}Ca with ^{237}Np, ^{243}Am, and ^{249}Bk undergo α decay. However, in the regions between N = 152, 162, and 184, there is minimal stability against SF for nuclei with N $\approx$ 157–159 and N $\approx$ 169–171. For these neutron numbers, odd-Z and odd-N nuclei can avoid SF through the double hindrance of an odd proton and an odd neutron.

Annu. Rev. Nucl. Part. Sci. 2013.63:383-405. Downloaded from www.annualreviews.org
Access provided by WIB6380 - Gesellschaft fur Schwerionenforschung on 11/10/20. For personal use only.

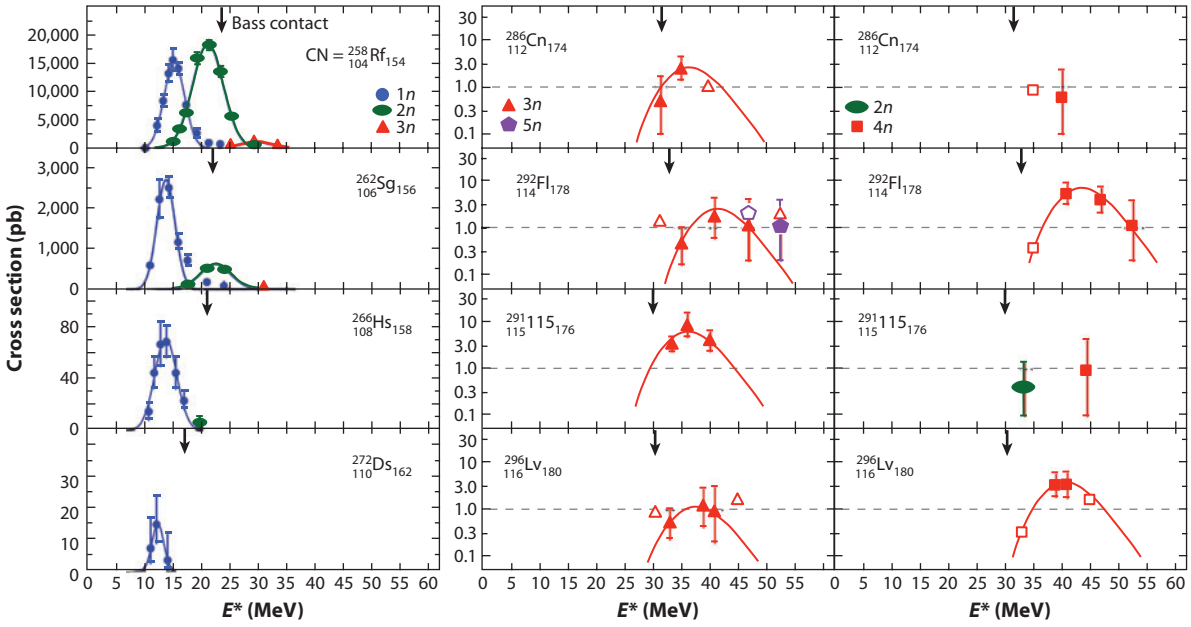

Figure 8

Cross sections and excitation functions measured in cold and hot fusion reactions. Open symbols represent cross-section limits. Gaussian curves were fitted to the data points measured in cold fusion reactions. A typical calculated evaporation function is drawn through the data points in the case of hot fusion reactions. Arrows indicate the excitation energy of compound nuclei obtained at beam energies just high enough for reaching a contact configuration, according to the fusion model by Bass (87).

6.3. Cross Sections and Excitation Functions

Figure 3 shows cross-section data for cold fusion reactions with ^{208}Pb and ^{209}Bi and for hot fusion reactions with actinide targets. The cold fusion cross sections decrease very sharply to element 113. The lowest production cross section, $\sigma_n = 22^{+20}_{-13}$ fb for element 113, was measured as three events during a 553-day bombardment of ^{209}Bi targets by ^{70}Zn projectiles (56). This value appears to be the limit in Z for cold fusion. The cross sections of hot fusion reactions with ^{48}Ca also decrease to Z = 110 but then rise again (**Figure 3**).

Excitation functions have been measured for cold and hot fusion reactions. In cold fusion reactions, the maximum EVR cross section (1*n* evaporation channel) was well below a one-dimensional fusion (Bass) barrier (87). By contrast, in hot fusion reactions, the excitation functions were located completely above the Bass contact configuration, which was calculated for a mean radius of the deformed target nucleus. The excitation curve for the hot fusion reaction for ^{292}114 and ^{291}115 had a width (full width at half maximum) of ~10 MeV, which is twice as broad as the 4.6-MeV width measured for ^{265}Hs. More importantly, the measured cross sections for hot fusion reactions of elements 114–118 range from 10 to 0.5 pb—orders of magnitude above the values expected from the decreasing trend of cross sections below element 110 for both hot and cold fusion (**Figure 3**). **Figure 8** shows examples of the experimental excitation functions for some cold and hot fusion reactions.

In cold fusion reactions at the optimum beam energy, the projectile and spherical target nuclei come to rest just when the outer orbits collide (**Figure 9**) (16). This configuration is obtained at energies even below the values where the mean radii reach a contact configuration, according to

Annu. Rev. Nucl. Part. Sci. 2013.63:383-405. Downloaded from www.annualreviews.org
Access provided by WIB6380 - Gesellschaft fur Schwerionenforschung on 11/10/20. For personal use only.

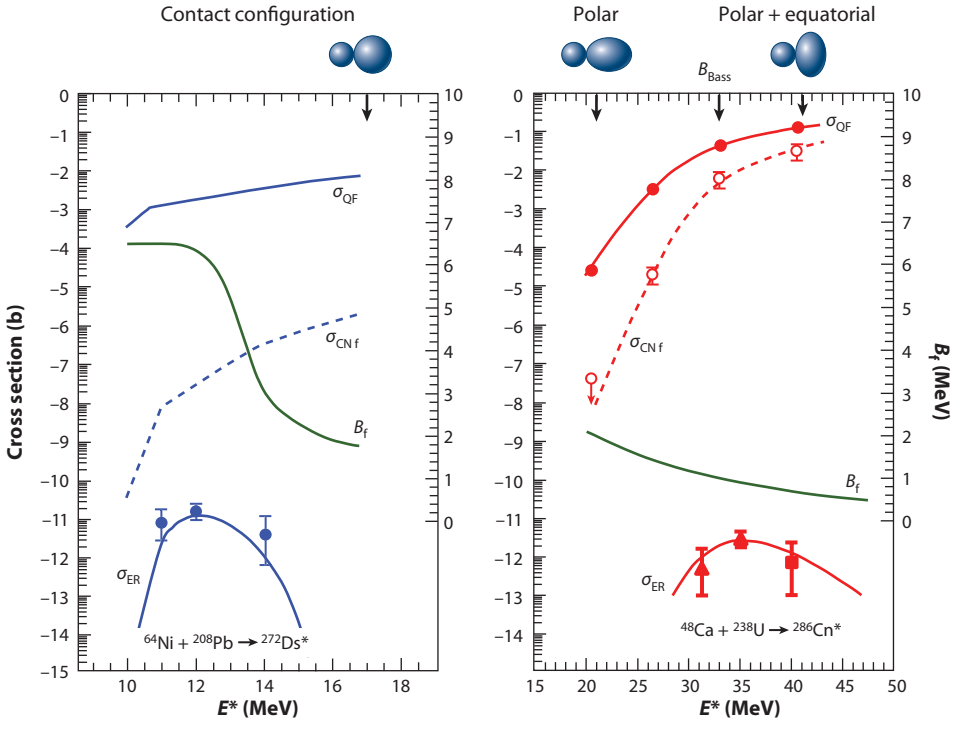

Figure 9

Cross sections for cold and hot fusion reactions. Experimental data are from Reference 43 and References 58 and 94 for cold and hot fusion reactions, respectively. Curves represent calculations from Reference 95 for cold fusion reactions and from Reference 96 for hot fusion reactions. Also shown are the heights B_f of the fission barriers as a function of the excitation energy, which was used in the model calculations. The arrow at top left indicates the excitation energy, which arises from a reaction at a beam energy that is just high enough to reach a contact configuration, according to the Bass model (87). The arrows on the right indicate the energies arising from the two contact configurations shown and for the Bass model, assuming a spherical target nucleus. Abbreviation: QF, quasi-fission.

the fusion model by Bass (87). The simple fusion barrier based on the Bass model is too high, and a tunneling process through the barrier cannot explain the measured cross sections. Various processes, such as transfer of nucleons and excitation of vibrational degrees of freedom, may decrease the fusion barrier.

At first glance, the situation seems quite different for hot fusion. The maximum of the excitation function is located well above the value needed to reach the Bass contact configuration. However, given the deformation of the target nuclei and fusion in the equatorial orientation (**Figure 9**), the projectile and target nuclei fuse from a starting configuration that is similar to that in cold fusion. The measured excitation functions also reveal that fusion at low beam energies that are just high enough to reach contact in an elongated configuration does not occur, despite the resulting low excitation energy (58, 88). It follows that for CN formation in actinide + ^{48}Ca reactions, the orientation of the target nuclei at the touching point is decisive. The hexadecapole deformation must also be considered (89–91).

Recent successful heavy-element syntheses have inspired several theoretical studies to obtain a detailed quantitative understanding of the reaction processes (92; also see the citations in

Annu. Rev. Nucl. Part. Sci. 2013.63:383-405. Downloaded from www.annualreviews.org
Access provided by WIB6380 - Gesellschaft fur Schwerionenforschung on 11/10/20. For personal use only.

Reference 16). For nuclei around ^{278}Cn produced in cold fusion, Pei et al. (93) predicted more rapid decrease of fission barriers with excitation energy, as compared with nuclei around ^{292}114 produced in hot fusion, as a consequence of the difference between ground-state and saddle-point temperatures. A study of SHN fission barriers that used a self-consistent nuclear density theory obtained this predicted result.

Figure 9 depicts examples of measured and calculated cross sections for quasi-fission, CN fission, and EVRs as a function of excitation energy along with B_f for the reactions shown for cold and hot fusion. **Figure 9** also shows the extreme smallness of the EVR cross sections relative to the total reaction cross section.

A quantitative estimate of fusion cross sections with radioactive ion beams (RIBs) was performed for cold and hot fusion reactions (97). Many of the cold fusion cross sections with RIBs of calcium to rubidium with one to nine more neutrons than those of their heaviest stable isotopes could be a factor of 20 higher than with stable beams. However, RIB intensities are much lower than for stable beams. Therefore, the measurement of reaction cross sections with RIBs will be an important study to undertake in the future.

7. NEAR PLANS AND FUTURE PROJECTS

7.1. Current and Future Experiments

Another experiment that aims to synthesize new isotopes of element 118 in $^{249-251}$Cf + ^{48}Ca reactions is being considered at FLNR. Presently, the only source of ^{251}Cf is 30–40-year-old material irradiated in HFIR to produce ^{252}Cf, in which the much longer lived $^{249-251}$Cf remain. A pure sample of ^{251}Cf will require mass separation of $^{249-251}$Cf. With such a target of mixed isotopes of californium, in 3*n* and 4*n* evaporation channels the three new isotopes—^{293}118, ^{295}118, and ^{296}118—could be produced. Note that ^{251}Cf is the heaviest nuclide that can be produced with HFIR in required amounts. For the synthesis of elements with $Z > 118$, projectiles of heavier ions, instead of ^{48}Ca, have to be used.

Using the TASCA separator, researchers at GSI searched for element 119 by using the reaction ^{249}Bk + ^{50}Ti between April and October 2012 (77). No event that could be assigned to the decay of an isotope of element 119 was found. The estimated sensitivity of the experiment corresponds to a cross section of ~55 fb for one detected event.

Other groups have attempted to synthesize element 120. Researchers at GSI SHIP studied the reactions ^{238}U + ^{64}Ni and ^{248}Cm + ^{54}Cr. For the ^{238}U + ^{64}Ni reaction, a 116-day run yielded an upper cross-section limit of 90 fb (98). The first ^{248}Cm + ^{54}Cr experiment yielded an upper limit of 560 fb over 33 days (99). Physicists at FLNR studied the reaction ^{244}Pu + ^{58}Fe and found an upper limit of 400 fb over 60 days (100). The reaction $^{249-251}$Cf + ^{50}Ti for the synthesis of element 120, which is also possible but technically more complicated, has not yet been studied. However, in this case as well, the cross section may drop to 20–50 fb or even lower. For the synthesis of elements with $Z \geq 119$, the experimental sensitivity should be significantly improved.

Now that improved, dedicated facilities that will provide higher beam intensities and detection sensitivities are being developed, researchers will study the extension to nuclei around the island of stability and thus the underlying shell effects, including more neutron-deficient isotopes. Spectroscopic data on lower-Z isotopes may allow the extraction of information about the shell structure of nuclei up to $Z = 126$, one of the predicted closed proton shells, even if such high-Z nuclei cannot be produced in experiments. Other important questions are how to produce more neutron-rich nuclei nearer to the island of stability at $N = 184$ and how to produce more neutron-rich isotopes of $Z = 107$–114, which are expected to have longer half-lives. Neither can be directly produced

Annu. Rev. Nucl. Part. Sci. 2013.63:383-405. Downloaded from www.annualreviews.org
Access provided by WIB6380 - Gesellschaft fur Schwerionenforschung on 11/10/20. For personal use only.

in fusion reactions by use of beams and targets of stable isotopes. Further studies are needed to determine whether SHN exist in nature, either from recent supernova explosions or in the Earth.

7.2. New Facilities

In the near future, FLNR plans to upgrade the U400 cyclotron for higher beam intensities and to improve the separator efficiency and luminosity of its experiments. FLNR is also in the process of constructing an SHN factory that could produce up to 1,000 SHN in a reasonable time. The building will have a new, higher-current cyclotron with 5–10 p μA of ^{48}Ca and a more efficient recoil separator. These advances will allow the opportunity to perform extensive studies of details of the structure of SHN through α and β decay, SF and fission modes, γ-ray spectroscopy, and mass measurements and will also enable research into the atomic structure and chemistry of superheavy elements.

In 2015, the GANIL laboratory in France will open new facilities to study SHN. The new Facility for Radioactive Beams, under development at Michigan State University, intends to use RIBs to study more neutron-rich SHN.

8. SUMMARY

The discoveries of elements 107–112 by cold fusion and elements 113–118 by hot fusion have been well established. Cross-bombardment verification, measurements of excitation functions, and reproducible results obtained at different laboratories were all important in establishing these discoveries.

The properties of the heaviest nuclei and their decay products with Z = 104–118 and N = 153–177, covering the mass range A = 257–294 (**Figure 2**), reveal that for nuclei whose Z is 40% greater than that of lead there exists an impressive extension in nuclear survivability. Although SHN are at the limits of Coulomb stability, shell stabilization lowers the ground-state energy, creates a fission barrier, and thereby enables SHN to exist. The basic theoretical concept of the existence of closed shells in the region of the hypothetical SHN and their decisive role in determining the limits of nuclear mass have been verified experimentally.

DISCLOSURE STATEMENT

The authors are not aware of any affiliations, memberships, funding, or financial holdings that might be perceived as affecting the objectivity of this review.

ACKNOWLEDGMENTS

J.H.H.'s work at Vanderbilt University was supported by the US Department of Energy through grant DE-FG-05-88ER40407. S.H.'s was supported by the Helmholtz Association through a Helmholtz Professorship. We acknowledge the support of the Russian Foundation for Basic Research through grants 11-02-12050 and 11-02-12066.

LITERATURE CITED

1. Strutinsky VM. *Nucl. Phys. A* 95:420 (1967)
2. Sobiczewski A, et al. *Phys. Lett.* 22:500 (1966)
3. Meldner H. *Ark. Fys.* 36:593 (1967)

Annu. Rev. Nucl. Part. Sci. 2013.63:383-405. Downloaded from www.annualreviews.org
Access provided by WIB6380 - Gesellschaft fur Schwerionenforschung on 11/10/20. For personal use only.

Annu. Rev. Nucl. Part. Sci. 2013.63:383-405. Downloaded from www.annualreviews.org
Access provided by WIB6380 - Gesellschaft fur Schwerionenforschung on 11/10/20. For personal use only.

4. Nilsson SG, et al. *Nucl. Phys. A* 115:545 (1968)
5. Mosel U, Greiner W. *Z. Phys.* 222:261 (1969)
6. Grumann J, et al. *Z. Phys.* 228:371 (1969)
7. Fiset EO, Nix JR. *Nucl. Phys. A* 193:647 (1972)
8. Randrup J, et al. *Phys. Rev. C* 13:229 (1976)
9. Smolanczuk R, et al. *Phys. Rev. C* 52:1871 (1995); Smolanczuk R, Sobiczewski A. In *Proceedings of the 15th Nuclear Divisional Conference on Low Energy Nuclear Dynamics*, ed. YS Oganessian, R Kalpachieva, p. 313. Singapore: World Sci. (1995)
10. Flerov GN, Ter-Akopian GM. *Rep. Prog. Phys.* 46:818 (1983)
11. Dechargé J, Gogny D. *Phys. Rev. C* 21:1568 (1980)
12. Berger JF, et al. *Nucl. Phys. A* 428:23c (1984); Berger JF, et al. *Nucl. Phys. A* 685:1c (2001)
13. Ćwiok S, et al. *Phys. Rev. Lett.* 82:1108 (1999)
14. Bender M, et al. *Phys. Rev. C* 58:2126 (1998); Bender M, et al. *Phys. Rev. C* 60:034304 (1999)
15. Sobiczewski A. *Radiochim. Acta* 99:395 (2011)
16. Hofmann S. *Radiochim. Acta* 99:405 (2011)
17. Oganessian YT. *Radiochim. Acta* 99:429 (2011)
18. Oganessian YT, et al. *J. Exp. Theor. Phys. Lett.* 20:265 (1974)
19. Flerov GN, Ter-Akopian GM. *Prog. Part. Nucl. Phys.* 19:197 (1987)
20. Münzenberg G, et al. *Nucl. Instrum. Methods* 161:65 (1979)
21. Hofmann S, et al. *Z. Phys. A* 291:53 (1979)
22. Hofmann S, Münzenberg G. *Rev. Mod. Phys.* 72:733 (2000)
23. Block M, et al. *Nature* 463:785 (2010)
24. Ninov V, et al. *AIP Conf. Proc.* 455:704 (1998)
25. Ellison PA, et al. *Phys. Rev. Lett.* 105:182701 (2010)
26. Morita K, et al. *Eur. Phys. J. A* 21:257 (2004)
27. Gan SZ, et al. *Eur. Phys. J. A* 20:385 (2004); Gan SZ, et al. *Eur. Phys. J. A* 10:21 (2001)
28. Düllmann ChE, et al. *Phys. Rev. Lett.* 104:252701 (2010)
29. Münzenberg G, et al. *Z. Phys. A* 300:107 (1981)
30. Münzenberg G, et al. *Z. Phys. A* 333:163 (1989)
31. Wilk PA, et al. *Phys. Rev. Lett.* 85:2697 (2000)
32. Eichler R, et al. *Nature* 407:63 (2000)
33. Münzenberg G, et al. *Z. Phys. A* 309:89 (1982)
34. Münzenberg G, et al. *Z. Phys. A* 330:435 (1988)
35. Hofmann S, et al. *Z. Phys. A* 358:377 (1997)
36. Nelson SL, et al. *Phys. Rev. C* 79:027605 (2009)
37. Münzenberg G, et al. *Z. Phys. A* 317:235 (1984)
38. Münzenberg G, et al. *Z. Phys. A* 324:489 (1986)
39. Hofmann S, et al. *Z. Phys. A* 350:277 (1995)
40. Türler A, et al. *Eur. Phys. J. A* 17:505 (2003)
41. Dvorak J, et al. *Phys. Rev. Lett.* 97:242501 (2006)
42. Oganessian YT, et al. *Phys. Rev. C* 87:034605 (2013)
43. Hofmann S. *Rep. Prog. Phys.* 61:639 (1998)
44. Ginter TN, et al. *Phys. Rev. C* 67:064609 (2003)
45. Zhang ZY, et al. *Chin. Phys. Lett.* 29:012502 (2012)
46. Hofmann S, et al. *Eur. Phys. J. A* 10:5 (2001)
47. Hofmann S, et al. *Z. Phys. A* 350:281 (1995)
48. Morita K, et al. *J. Phys. Soc. Jpn.* 73:1738 (2004)
49. Folden CM III, et al. *Phys. Rev. Lett.* 93:212702 (2004)
50. Hofmann S, et al. *Z. Phys. A* 354:229 (1996)
51. Hofmann S, et al. *Eur. Phys. J. A* 14:147 (2002)
52. Morita K, et al. *J. Phys. Soc. Jpn.* 76:043201 (2007)
53. Hofmann S, et al. *GSI Sci. Rep.* 2003:1 (2003); Hofmann S, et al. *GSI Sci. Rep.* 2004:1 (2004)
54. Morita K, et al. *J. Phys. Soc. Jpn.* 73:2593 (2004)

55. Morita K, et al. *J. Phys. Soc. Jpn.* 76:045001 (2007)
56. Morita K, et al. *J. Phys. Soc. Jpn.* 81:103201 (2012)
57. Minaya Ramirez E, et al. *Science* 337:1207 (2012)
58. Oganessian YT, et al. *Phys. Rev. C* 70:064609 (2004)
59. Oganessian YT, et al. *Phys. Rev. C* 62:041604 (2000); Oganessian YT. *Phys. At. Nucl.* 63:1679 (2000)
60. Oganessian YT, et al. *Phys. Rev. C* 69:054607 (2004)
61. Dmitriev SN, et al. *Mendeleev Commun.* 15:1 (2005)
62. Stoyer NJ, et al. *Nucl. Phys. A* 787:388c (2007)
63. Oganessian YT, et al. *Phys. Rev. C* 63:011301 (2001); Oganessian YT, et al. *Phys. At. Nucl.* 64:1349 (2001)
64. Oganessian YT, et al. *Phys. Rev. C* 74:044602 (2006)
65. Hofmann S, et al. *Eur. Phys. J. A* 32:251 (2007)
66. Hofmann S, et al. *Eur. Phys. J. A* 48:62 (2012)
67. Oganessian YT, et al. *Joint Institute for Nuclear Research Communication D7-2002-287*. Dubna, Russ.: Jt. Inst. Nucl. Res. (2002); Oganessian YT, et al. *Lawrence Livermore National Laboratory Report UCRL-ID-151619*. Livermore, Calif.: Lawrence Livermore Natl. Lab. (2002)
68. Oganessian YT, *Phys. Scr.* 125:57 (2006)
69. Oganessian YT, et al. *Phys. Rev. Lett.* 109:162501 (2012)
70. Oganessian YT, et al. *Phys. Rev. C* 69:021601 (2004)
71. Oganessian YT, et al. *Phys. Rev. C* 72:034611 (2005)
72. Oganessian YT, et al. *Phys. Rev. Lett.* 108:022502 (2012)
73. Oganessian YT, Abdullin FS. *Phys. Rev. C* 87:014302 (2013)
74. Hamilton JH, et al. In *Proceedings of the International Conference on Nucleus–Nucleus Collisions. J. Phys. Conf. Ser.* 420:012011 (2013)
75. Oganessian YT, et al. *Phys. Rev. Lett.* 104:132502 (2010)
76. Oganessian YT, et al. *Phys. Rev. C* 83:054315 (2011)
77. Düllmann CE. In *Proceedings of the 5th International Conference on Fission and Properties of Neutron-Rich Nuclei*, ed. JH Hamilton, AV Ramayya. Singapore: World Sci. In press (2013)
78. Eichler R, et al. *Nature* 447:72 (2007)
79. Eliav E, et al. *Phys. Rev. A* 52:2765 (1995); Seth M, Schwerdtfeger P, Dolg M. *J. Chem. Phys.* 106:3623 (1997)
80. Pershina V, et al. *Radiochim. Acta* 94:181 (2006)
81. Pitzer S. *J. Chem. Phys.* 63:1032 (1975)
82. Düllmann CE, et al. *Nucl. Instrum. Methods A* 479:631 (2002); Soverna S, et al. *Radiochim. Acta* 93:1 (2005)
83. Eichler R, et al. *Nature* 447:72 (2007)
84. Muntian I, et al. *Acta Phys. Polon. B* 34:2073 (2003); Muntian I, et al. *Phys. At. Nucl.* 66:1015 (2003)
85. Sobiczewski A. *Acta Phys. Polon. B* 41:157 (2010)
86. Warda M, Egido JL. *Phys. Rev. C* 86:014322 (2012)
87. Bass R. *Nucl. Phys. A* 231:45 (1974)
88. Oganessian YT. *J. Phys. G* 34:R165 (2007)
89. Iwamoto A, et al. *Nucl. Phys. A* 596:329 (1996)
90. Misicu S, Greiner W. *Phys. Rev. C* 66:044606 (2002)
91. Fazio G, et al. *Eur. Phys. J. A* 19:89 (2004)
92. Siwek-Wilczynska K, et al. *Phys. Rev. C* 86:014611 (2012)
93. Pei JC, et al. *Phys. Rev. Lett.* 102:192501 (2009)
94. Itkis MG, et al. In *Proceedings of the International Workshop on Fusion Dynamics at the Extremes*, ed. VI Zagrebaev, p. 93. Singapore: World Sci. (2001)
95. Giardina G, et al. *Eur. Phys. J. A* 8:205 (2000)
96. Zagrebaev VI, et al. *Phys. At. Nucl.* 66:1033 (2003)
97. Loveland W. *Phys. Rev. C* 76:014612 (2007)
98. Hofmann S, et al. *GSI Sci. Rep.* 2009:131 (2009)
99. Hofmann S, et al. *GSI Sci. Rep.* 2012:205 (2012)
100. Oganessian YT, et al. *Phys. Rev. C* 79:024603 (2009)

Annu. Rev. Nucl. Part. Sci. 2013.63:383-405. Downloaded from www.annualreviews.org
Access provided by WIB6380 - Gesellschaft fur Schwerionenforschung on 11/10/20. For personal use only.

Annual Review of Nuclear and Particle Science

Volume 63, 2013

Contents

Annu. Rev. Nucl. Part. Sci. 2013.63:383-405. Downloaded from www.annualreviews.org
Access provided by WIB6380 - Gesellschaft fur Schwerionenforschung on 11/10/20. For personal use only.

Index

Errata

An online log of corrections to *Annual Review of Nuclear and Particle Science* articles may be found at http://nucl.annualreviews.org/errata.shtml

Annu. Rev. Nucl. Part. Sci. 2013.63:383-405. Downloaded from www.annualreviews.org
Access provided by WIB6380 - Gesellschaft fur Schwerionenforschung on 11/10/20. For personal use only.